V International Conference on Computational Methods for Coupled Problems in Science and Engineering
COUPLED PROBLEMS 2013
S. Idelsohn, M. Papadrakakis and B. Schrefler (Eds)

# FSI OF HIGH PERFORMANCE HIGH-LIFT DEVICES WITH CIRCULATION CONTROL VIA CONDITIONED COANDĂ-JETS

**KAY SOMMERWERK, MATTHIAS C. HAUPT AND PETER HORST**

Institute of Aircraft Design and Lightweight Structures (IFL)
TU Braunschweig
Herrmann-Blenk-Str. 35, 38106 Braunschweig, Germany
e-mail: k.sommerwerk@tu-braunschweig.de, web page: http://www.tu-braunschweig.de/ifl

**Key words:** High-Lift, Coandă effect, Circulation Control, Aerodynamic performance, Fluid-structure interaction

**Abstract.** Current transport aircraft are limited to airports with comparatively long runways for take-off and landing. An aircraft with short take-off and landing capabilities is under investigation at the Collaborative Research Center 880. The aircraft employs circulation controlled high lift devices where high velocity air is blown through a slot in front of the flap. These high performance high-lift devices allow take-off and landing of the aircraft at runways of 800 m length. The curved flap leading edge induces a Coandă effect with the jet resulting in an attached flow up to the tip of the flap even at high deflection angles of up to 85°. Examination of the aeroelasticity of the wing is of high importance because of the sensitivity of the Coandă effect to perturbation through deformation and consequential change in flow.

The large pressure gradients can play a significant role in the effective use of this jet system. Preliminary studies have shown an influence on aerodynamic performance due to slot deformation. Small changes in the aerodynamic characteristics can have adverse effects on the stall behavior. A flap section model of the wing is used to analyze the performance for several flight states. This high detail model allows capturing fine effects over the whole wing chord and on the slot region while still including wing deformations.

The aerodynamic performance of the aeroelastic flap section model is compared to the characteristics of the rigid airfoil. The analyzed flight states give an insight into the influence of the deformation on the flow. Additionally the effects of jet momentum variation on aerodynamics is shown and the dominant stall phenomena presented. The local relative change in pressure can reach values between 10 and 20 % and has an influence on the stall behavior of the section. The change in aerodynamic performance illustrates the influence of small deformations on the sensitive circulation control.

## 1 INTRODUCTION

Airfoils employing high lift systems with circulation control have shown very high lift coefficient values of up to 5.2 for 2D analyses [1]. The collaborative research center SFB 880 investigates an aircraft which is distinguished through short take-off and landing capabilities by making use of the Coandă effect. High velocity air is blown through a slot directly upstream of a deflected plain flap. This jet interacts with the boundary layer and induces a Coandă effect which keeps the flow attached to the high-lift device allowing high deflection angles of up to 85°. Figure 1 displays the 100 passenger high wing monoplane with an engine bleed air system to generate the pressurized air for the flap jets. Other configurations that integrate compressor systems for each flap are also under investigation. The aeroelastic phenomena of wings with blown air configurations are of high importance to the overall aerodynamic performance of the aircraft, as they can deviate from the phenomena of conventional wings. Different stall phenomena have been identified which depend on the jet performance. The jet performance is dependent on the deformation of the duct system due to the pressurized air in the duct as well as due to the wing deformation because of aerodynamic loads. The slot height in comparison to the overall model dimensions lies in the order of magnitude of $10^{-3}$ therefore requiring high resolution structural and aerodynamic models for the analyses.

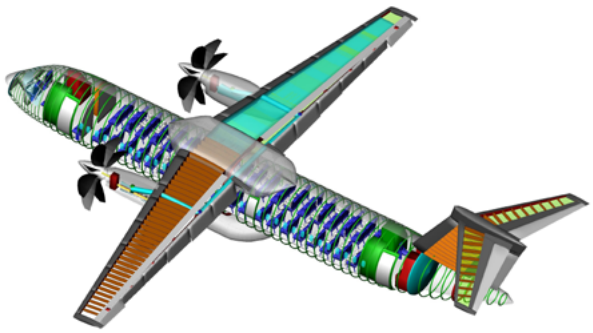

**Figure 1**: SFB 880 reference aircraft [2]

The presented study gives insight into the overall aerodynamic performance of a flap sectional model under aeroelastic behavior. The stall phenomena of a Coandă flap are presented and the different jet performances for static airfoils are shown. One configuration from previous aeroelastic studies has been chosen for analyses of the stall behavior [3]. The flap sectional model is deformed via CFD-CSM coupling and the resulting performances are computed for several configurations with varying angle of attack and momentum coefficient.

## 2 MODELS

### 2.1 Structure

A flap sectional model as displayed in Fig. 2(a) is used for high detail analyses. Because of the low taper ratio of 0.38 of the aircraft wing the flap sectional model is untapered, which has a negligible effect on the accuracy on the analyses. The mean aerodynamic chord of the wing of 3.428 m is used as the chord length of the model. The flap width is 2.142 m and the slot height is 0.061 % of the chord length. The model is fixed with

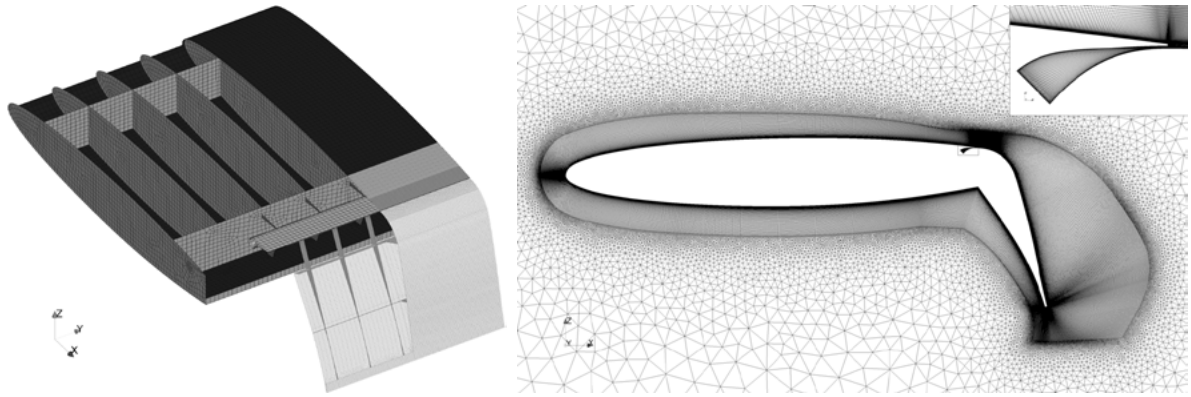

(a) Structural grid (b) Fluid grid

**Figure 2**: Computational grids

connecting boundary conditions on the inside rib. The cutting loads of the unrepresented outer wing are applied to the outboard rib. The model uses the external duct integration configuration with a slot stiffener distance of 102 mm [3]. A layered composite is employed for the material model and sizing is performed based on a fully stressed approach adapted for composites [3]. The aerodynamic surface loads are computed via CFD analyses and are transfered to the structure via the *ifls*-coupling environment [4]. The ANSYS solver is used for the structural analyses.

### 2.2 Aerodynamics

The 2D section of the fluid grid including a slot detail is shown in Fig. 2(b). It is a hybrid grid designed to capture the aerodynamic effects on the flap and includes a concave section for the air duct system. The grid is extruded in the spanwise direction 160 times for the required resolution. The extruded grid consists of 28 million points with 85 % of cells in the structured boundary layer. The aerodynamic computations are conducted with the TAU code 2011.2 of the German Aerospace Center (DLR), to solve the Reynolds-averaged Navier-Stokes equations (RANS) [5].

### 2.3 Coupling

The fluid structure interaction (FSI) process uses a partitioned approach to solve the fluid and structural problem. After solving the fluid problem for a given displacement the resulting boundary conditions are applied to the structure grid, which in turn alters the fluid grid through its computed deflection. In detail the pressure distribution on the wetted surface after reaching steady state in the CFD analysis is integrated to obtain the forces on each node of the fluid grid. These forces are transferred conservatively to the structure resulting in force vectors on the structural nodes. A FEM simulation is performed to obtain the nodal displacements, which can be used for stress-strain analyses

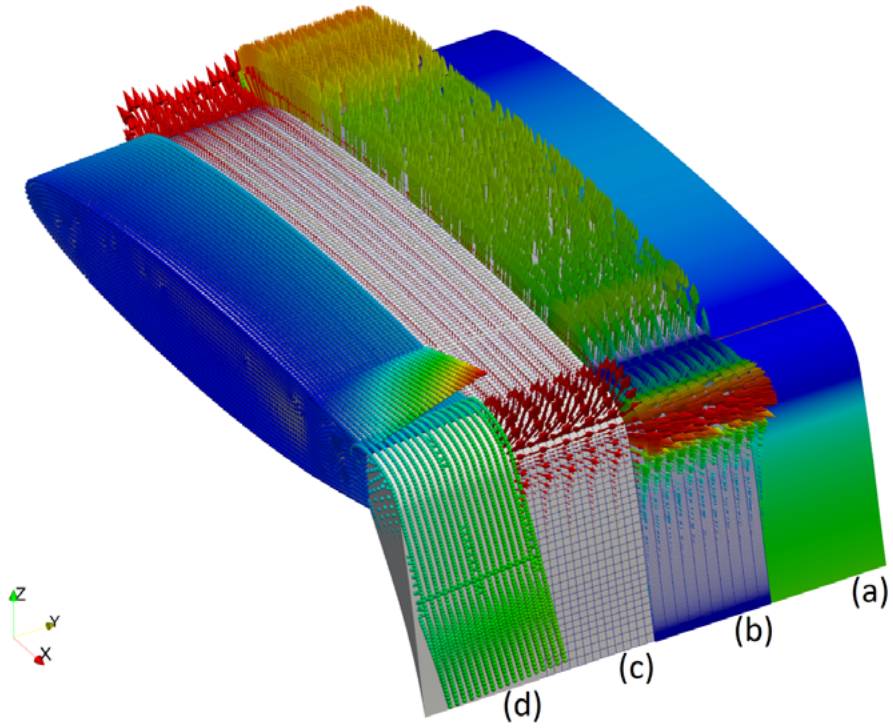


Figure 3: Flap section coupling process, (a) pressure distribution of the wetted aerodynamic surface, (b) integrated force vectors, (c) transfered force vectors on structural grid, (d) structural nodal displacements

or fluid grid deformation.

Figure 3 illustrates the coupling process over the span of the flap section. Figure 3(a) illustrates the pressure distribution of the wetted aerodynamic grid which is then integrated to the resulting force vectors shown in Fig. 3(b). The forces are transfered to the structural grid via the coupling environment resulting in the load vectors on the structural grid Fig. 3(c). Solving the finite element model with the imposed loads results in the nodal displacements in Fig. 3(d) used for sizing and mesh deformation.

## 3 Coandă effect and momentum coefficient

The circulation controlled high lift system makes use of the Coandă effect to mitigate flow separation at high flap deflection angles. The desired effect is an interaction of a blown jet directly upstream of the flap with the oncoming flow. The boundary layers intermix and the oncoming flow is accelerated. The high velocity jet flows by the curved flap leading edge, where a pressure gradient is induced because of the Coandă effect. Due to the low pressure on the flap surface the jet stays attached and is bend around the flap leading edge. The jet characteristic can be expressed dimensionless with the dynamic pressure of the flow to attain the momentum coefficient $c_\mu$.

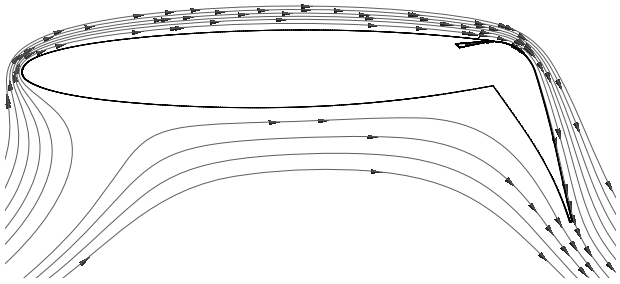

**Figure 4**: Dependence of $c_L$ on $c_\mu$

**Figure 5**: Nominal flow, $c_\mu = 0.06,\ \alpha = -2°,\ \delta = 65°$

It is defined as

$$c_\mu = \frac{\dot{m}_{jet} v_{jet}}{S_{ref} q_{\inf}} \tag{1}$$

where $\dot{m}_{jet}$ is the mass flow through the jet exit section and $v_{jet}$ is the velocity of the jet at the slot. $S_{ref}$ is the reference surface, which is the chord length multiplied by the span-wise flap length. The dynamic pressure $q_{\inf}$ is defined as

$$q_{\inf} = \frac{1}{2} \rho_{\inf} v_{\inf}^2 \tag{2}$$

with the density $\rho_{\inf}$ and the velocity $\rho_{\inf}$ of the flow.

The momentum coefficient is used as an indicator of jet performance. With an increase in $c_\mu$ the flow separates later from the flap resulting in increased lift. Figure 4 illustrates the jet performance to lift correlation. The increase in lift is linear to the increase in $c_\mu$ up to the point where the flow is attached on the entire flap. This point is optimal with respect to power consumption to generate the jet and increase in lift. Further increases in $c_\mu$ cause considerably lower lift increments. The flow around the airfoil with optimal $c_\mu$ is illustrated in Fig. 5 for a flap deflection of 65°, an angle of attack of −2° and a $c_\mu$ of 0.06. The jet intermixes with the oncoming flow and has enough momentum to reach the trailing edge. Leading edge stall for this configuration occurs at angles of attack of 3°. Note the stagnation point at about 20 % chord for the airfoil. Droop nose configurations are under investigation which move the stagnation point closer to the leading edge, thus raising the stall point 15°.

## 4 RESULTS

### 4.1 Stall phenomena

Because of the additional parameter $c_\mu$ the stall phenomena of an circulation controlled airfoil are more complex. An increase in $c_\mu$ does not always have a positive effect on lift and the result depends also on the angle of attack $\alpha$ and the flap deflection angle $\delta$. Considering a fixed flap deflection angle of 65° the occurring stall behavior is shown in

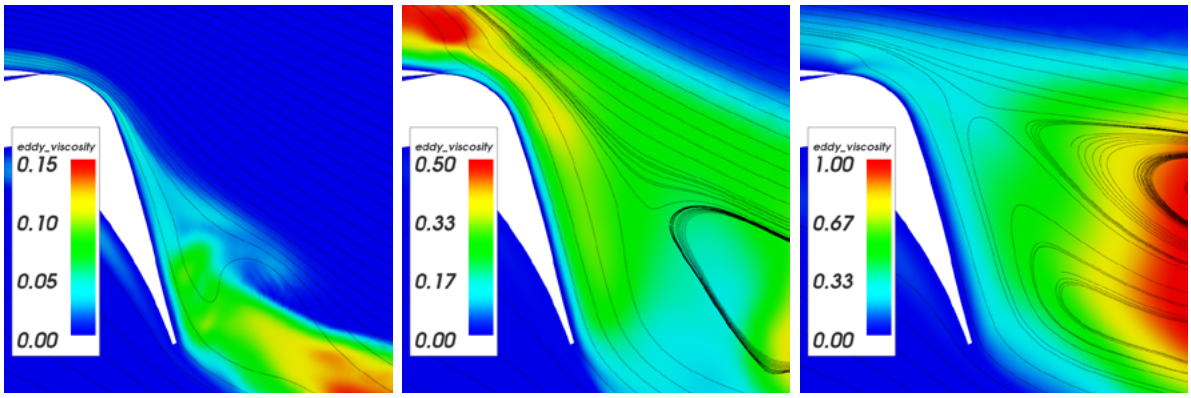


(a) Type I, $c_\mu = 0.0361,\ \alpha = 7°$ (b) Type II, $c_\mu = 0.06,\ \alpha = 5°$ (c) Type III, $c_\mu = 0.06,\ \alpha = 7°$

Figure 6: Stall phenomena of Coandă flap illustrated with stream lines and Spalart-Allmaras eddy viscosity

Fig. 6(a)–(c). Figure 6(a) shows the case of low momentum coefficient and is designated as type I stall . Here the jet and the outer flow mix effectively. However the flow separates before reaching the flap trailing edge as it has not enough momentum to overcome the adverse pressure gradient. With an increase of $c_\mu$ into the region of supercirculation the flow detaches at the leading edge of the airfoil thus leading to stall at lower angles as shown in Fig. 6(b). This is due to the increase in boundary layer thickness, which can not be caught entirely by the jet. Additionally, the large pressure gradient on the leading edge induced by the Coandă effect results in separation. Only small parts of the detached flow can be reattached to the flap. This stall is denoted as type II. A complete flow separation is denoted Type III stall. Here only a very thin part of the boundary layer stays attached. The jet momentum is to large to adequately mix with the boundary layer which changed with the angle of attack. Most of the flow detaches at the Coandă surface. This stall type does not necessarily include leading edge stall. Note in Fig. 6(c) the streamlines from the flap trailing edge up to the Coandă surface due to the adverse pressure gradients.

These phenomena show the sensitivity of the flow to the jet characteristics. Variation of the airfoil and slot geometry due to aeroelasticity not only influence the outer flow but can also affect the momentum coefficient as the jet velocity decreases with constant mass flow at higher slot cross sectional area.

### 4.2 Rigid airfoil characteristics

For reference the aerodynamic performance of the undeformed airfoil was evaluated for different angles of attack and different moment coefficients. The results are presented in Figure 7(a)–(c), with variable scale for the eddy viscosity computed with the on equation Spalart-Allmaras turbulence model [6]. The maximum lift coefficient $c_{L,max}$ is attained at the maximum $c_\mu$ at an angle of attack of 1°. It is evident, that for decreasing $c_\mu$ the value of $c_{L,max}$ decreases. Additionally the angle at which $c_{L,max}$ is attained increases.

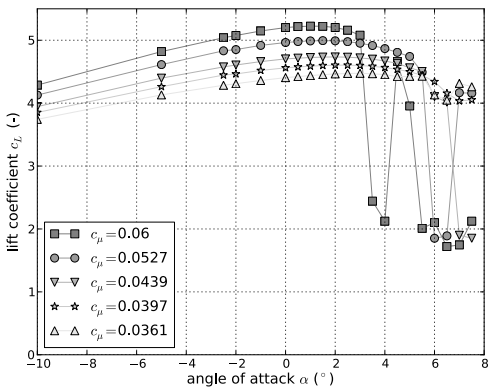


(a) Lift coefficient $c_L$

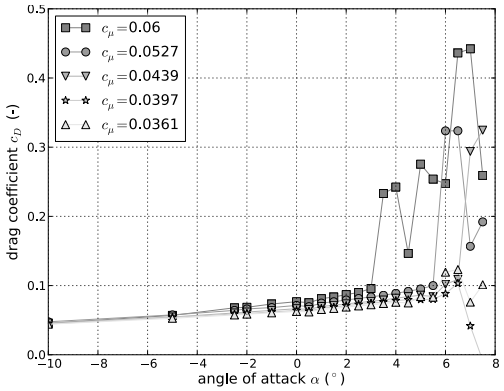


(b) Drag coefficient $c_D$

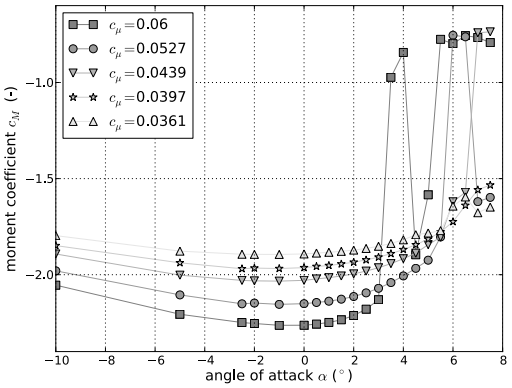


(c) Moment coefficient $c_M$

**Figure 7**: Aerodynamic coefficients $c_L, c_D, c_M$ as a function of $\alpha$ and $c_\mu$ of rigid airfoil

The stall behavior for high $c_\mu$ values are first type II and then type III. It can clearly be seen that at higher angles of attack, the flow might briefly reattach itself. This is the range where the stall changes from type II to III. At stall the lift coefficient drops to values around 2. The increase in drag and decrease in pitching moment as depicted in Fig. 7(b) and Fig. 7(c) is evident. Decreasing the moment coefficient reduces the induced pressure gradients at the leading edge which allows for later occurrence of type II and III stall. However parts of the flow detach before reaching the flap trailing edge because of the adverse pressure gradients. Part I stall does not have the severe effects as part II and III as the lift coefficient is only decreased marginally. The increase in drag and the decrease in pitching moment are fitting for the early separation and decreased lift.

### 4.3 Deformed airfoil

The deformation of the flap section due to the aerodynamic loads leads to a change in the pressure distribution on the section. Exemplary data for one x-z-slices of the profile at a spanwise location of 1.2 meters is shown in Fig. 8(a)–(d). Figure 8(a) displays the

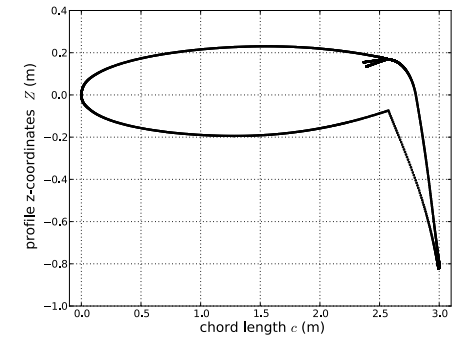


(a) Undeformed profile slice

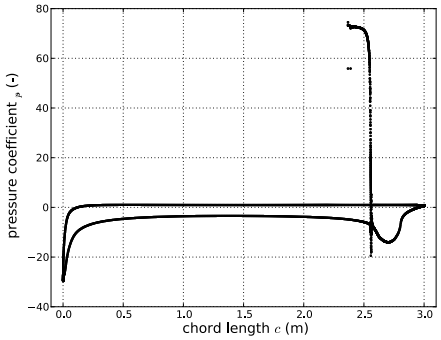


(b) $c_p$ distribution of undeformed profile

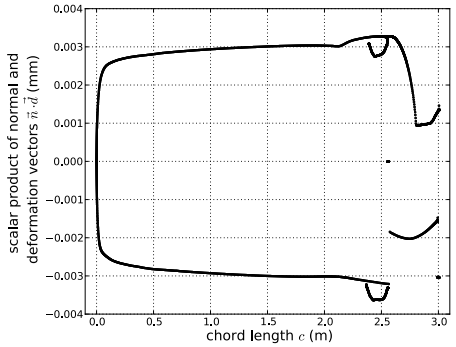


(c) Z-Displacement of slice

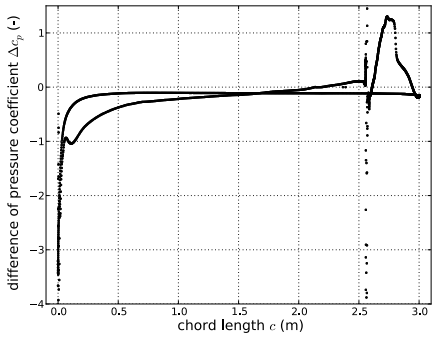


(d) Change in $c_p$

**Figure 8**: Profile slice of deformation and pressure distribution for $c_\mu = 0.06,\ \alpha = -0.25$

profile contour and Fig. 8(b) shows the respective displacement vector multiplied with the surface normals. The normals are computed on the surface elements and transfered to the grid points. Because of the change in sign of the normal vector, the displacement of the lower skins are depicted negative. Note the relative small displacements compared to the models dimensions, which are due to high stiffness of this section because of the inside position of this section on a real wing. From the leading edge to the spoiler at 2.1 m the model has a uniform displacement. It is slightly rotated around the y-axis. The higher offset points between 2.1 m and 2.55 m are the spoiler displacement and the displacement of the duct sheets due to the large jet outlet pressure. Again note the inversed normal for the lower sheet. The flap displacement coherently offset due to the rotation around the attachments to the wing box. Stray points are due to the interpolated normals on edges and corners of the airfoil.

The corresponding pressure distribution over the flap is shown in Fig. 8(c). Notable are the low pressures at the suction tip and over the Coandă surface. The mean $c_p$ over the top surfaces is close to -4. The lower side pressure coefficient has an almost constant value of 1. Notable again is the very high pressure coefficient of around 70 inside the jet duct .

Figure 8(d) displays the change in $c_p$-distribution due to the deformation. An overall change of -0.1 is recognizable on the lower surface including the flap. While the low values of pressure coefficient are reduced on the Coandă surface, the pressure is lowered at the nose. The relative change in pressure coefficient is about 10 % for the lower surface and leading edge, which linearly transitions to 0 % at the spoiler. The difference linearly increases to 24 % up to 2.9 m on the flap top surface.

It is evident, that the small deformations of a rather stiff section have a noticeable impact on the pressure distribution and thus the aerodynamic performance. A variation in pitching moment is also evident through the distribution differences shown in Fig. 8(d).

### Flexible section characteristics

The aeroelastic effect on the aerodynamics is investigated for the three highest momentum coefficients for several selected angles of attack. The angles where chosen around the interesting stall points. The lower momentum values in the domain of sub circulation are of low interest since stall type II and III occurs at higher angles than considered.

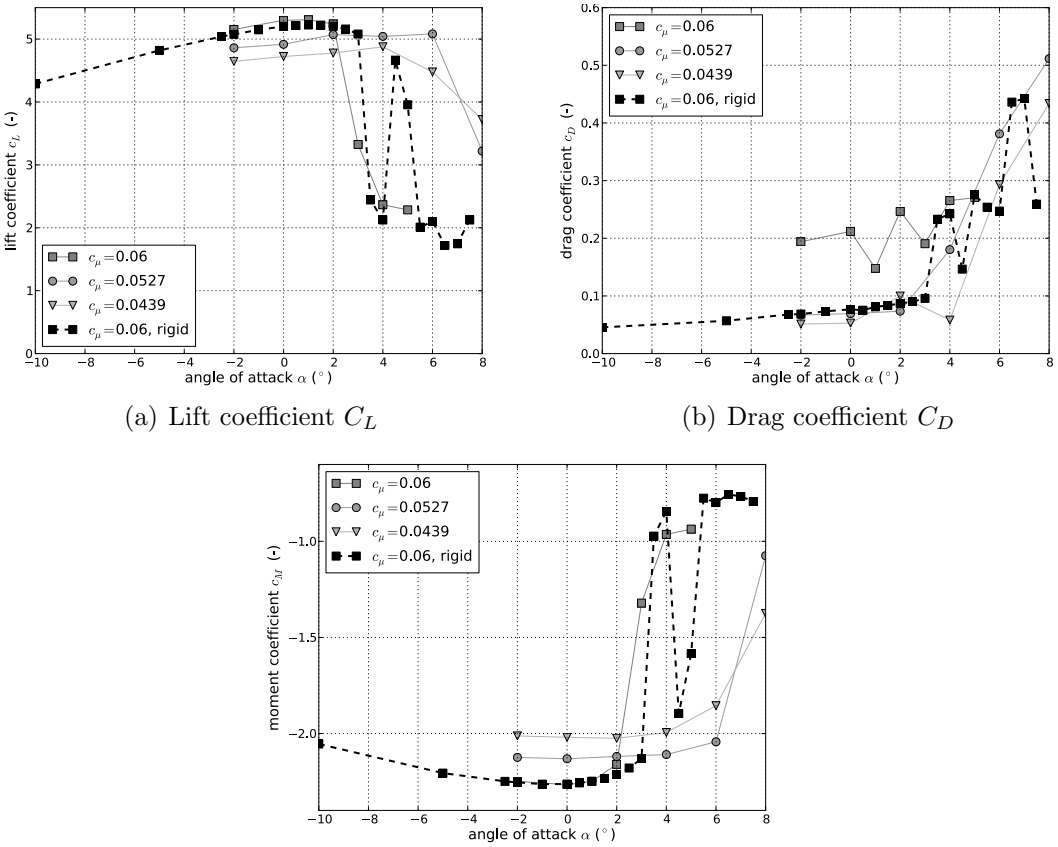


(a) Lift coefficient $C_L$

(b) Drag coefficient $C_D$

(c) Moment coefficient $c_M$

**Figure 9**: Aerodynamic coefficients $c_L, c_D, c_M$ as a function of $\alpha$ and $c_\mu$ for aeroelastic section

The results of the integrated variables are shown in Fig. 9(a)–(c) including the values of the rigid grid for $c_\mu = 0.06$. Examining the lift for $c_\mu = 0.06$ in the domain of super circulation as shown in Fig. 9(a) stall occurs at a lower angle of attack which is due to earlier leading edge separation.

This is confirmed by higher lift values of about 3 %, which induce early leading edge stall. The pitching moment coefficient reflects the stall behavior, though the same values are reached at later angles than on the undeformed model. While the drag before is double the drag of the undeformed airfoil, the drag is about 10 % higher on the deformed model during stall. This increase can be explained by the expansion of the wake, which is due to the splitting of the attached flow into an attached and detached part. This splitting occurs after the flow bent around the Coandă surface. One part stays attached and one part separates expanding the wake as shown in Fig. 10.

For the two other configurations which are in the nominal circulation range stall is delayed for one degree. The lift is increased in the same range as for $c_\mu = 0.06$ before stall. Stall occurs with a partial separation on the flap leading to higher lift over values of 3. The partial separation results in higher drag values during stall. The pitching moment reflects this behavior by reaching higher negative coefficients due to the existing lift on the Coandă surface.

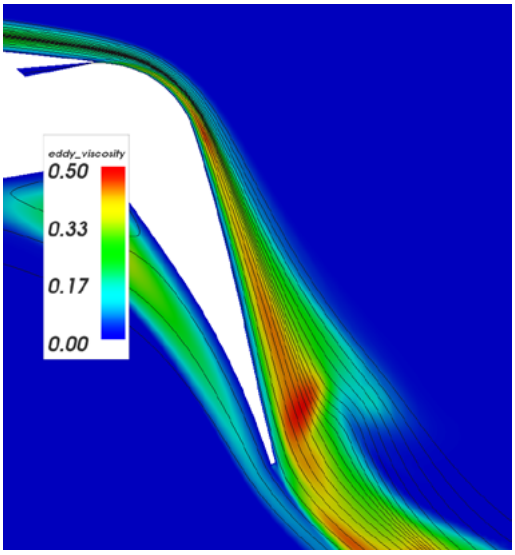


Figure 10: Wake expansion on flap illustrated with stream lines and Spalart-Allmaras eddy viscosity

It is evident, that even small deformations of the section have an impact on the variation of integrated aerodynamic variables. The overall change in lift is negligible, while the increase in drag due to partial separation over the flap as well as the change in pitching moment needs possibly be taken into account for flight dynamics. The stall point varies around 1 % illustrating the sensitivity of the circulation control to small airfoil variations. The stability changes depending on the moment coefficient and thus the circulation control domain. It is important to fully understand the change of stall points and phenomena in all three circulation control domains to be able to adapt the flight dynamics strategies and flight envelope accordingly.

## 5 CONCLUSIONS

In this paper we presented the influence of an elastic Coandă flap section on aerodynamic performance. A coupled flap section model was used to determine the deformations of the fluid grid for several momentum coefficients and angles of attack. Stall phenomena and aerodynamic characteristics of an rigid airfoil with blown air system were explained.